Tectonophysics 708 (2017) 56–69

Contents lists available at ScienceDirect

Tectonophysics

journal homepage: www.elsevier.com/locate/tecto

Change in the pattern of crustal seismicity at the Southern Central Andes from a local seismic network

Silvina Nacif [a,b,*], Marianela Lupari [b], Enrique G. Triep [a], Andrés Nacif [a], Orlando Álvarez [a,b], Andrés Folguera [b,c], Mario Gímenez [a,b]

[a] Instituto Geofísico Sismológico F. Volponi, Universidad Nacional de San Juan, Ruta 12, Km 17, Marquesado, Rivadavia, San Juan, Argentina
[b] Consejo Nacional de Investigaciones Científicas y Técnicas, Conicet, Argentina
[c] Instituto de Estudios Andinos, Departamento de Ciencias Geológicas, Universidad Nacional de Buenos Aires, Argentina

ARTICLE INFO

Article history:
Received 21 October 2016
Received in revised form 3 April 2017
Accepted 11 April 2017
Available online 17 April 2017

Keywords:
Southern Central Andes
Crustal seismicity
Andean growth
Erosion
Fore-arc and intra-arc and back-arc

ABSTRACT

Shallow seismicity in the Southern Central Andes is associated with interplate earthquakes due to the subduction of the Nazca plate beneath the South American plate and neotectonic activity, mainly located in the retro-arc region. However, this pattern changes drastically south of 34°S within the transition zone at the Southern Central Andes where crustal seismicity associated with mountain-building processes concentrates at the fore-arc and intra-arc region. In order to define more accurately this transition we used data from a high density-seismic network over the Chilean fore-arc and axial Andean sector (~33–34.5°S). We obtained a constraint data set of 77 seismic events located mostly in the Principal Cordillera western flank in the first 10 km of the upper crust. This cluster implies an abrupt change in the pattern of seismicity at the Southern Central Andes with a set of structures in the fore-arc and intra-arc accommodating shortening. This change in the locus of crustal seismicity and particularly its location on the fore-arc and intra-arc south of 34°S is discussed on the light of different hypotheses among which changes in the precipitation pattern and erosion along the Andes were favored. Focalized erosion associated with direction of prevailing Pacific winds south of ~34°S could determine subcritical conditions that could be adjusted by out-of-sequence deformation causing crustal earthquakes in the fore-arc region, becoming the retro-arc zone nearly fossilized from a deformational point of view. Additionally, trench sediments associated with this change in the precipitation pattern could also favor decoupling of the subduction zone inhibiting retro-arc seismicity, although it does not explain activation of fore-arc structures south of 34°S and their absence north of this latitude. Finally, inhomogeneous distribution of seismicity through the fore-arc zone south of 34°S is discussed on the light of variable elastic thicknesses.

© 2017 Elsevier B.V. All rights reserved.

1. Introduction

Crustal seismicity across the Andes, the longest and highest subduction-related orogen on Earth, denotes active mountain building activity and therefore has been a matter of interest and analysis through time (Isacks et al., 1982). Intraplate shallow seismicity exhibits low magnitudes and its occurrence is less frequent than in giant underthrusting events which occur in the interface between the subducted oceanic lithosphere and the overriding plate. Due to that most of the attention has been paid to this stronger seismicity with rupture areas reaching hundreds of kilometers, widespread strong shaking, and destructive tsunamis, distribution and occurrence of crustal earthquakes are not fully understood along the Andes yet (Christensen and Ruff, 1986; Beck et al., 1998; Moreno et al., 2009; Lange et al., 2012; Ruiz et al., 2013; among others).

Crustal seismicity, its distribution and main patterns allow establishing segmentation related to mountain building processes independently to that of giant earthquakes in the subduction zone. In particular, crustal seismicity between ~33°S and 35.5°S through the Southern Central Andes (Gansser, 1973) experiences a shift in locus between patches of concentrations on the eastern Andean foothills in the north and clusters implanted in the fore-arc and intra-arc region in the south (Fig. 1).

* Corresponding author at: Ruta 12 Km 17, Jardín de los Poetas, Marquesado, Rivadavia, San Juan C.P. 5407, Argentina.
E-mail address: nacif.silvina@gmail.com (S. Nacif).

http://dx.doi.org/10.1016/j.tecto.2017.04.012
0040-1951/© 2017 Elsevier B.V. All rights reserved.

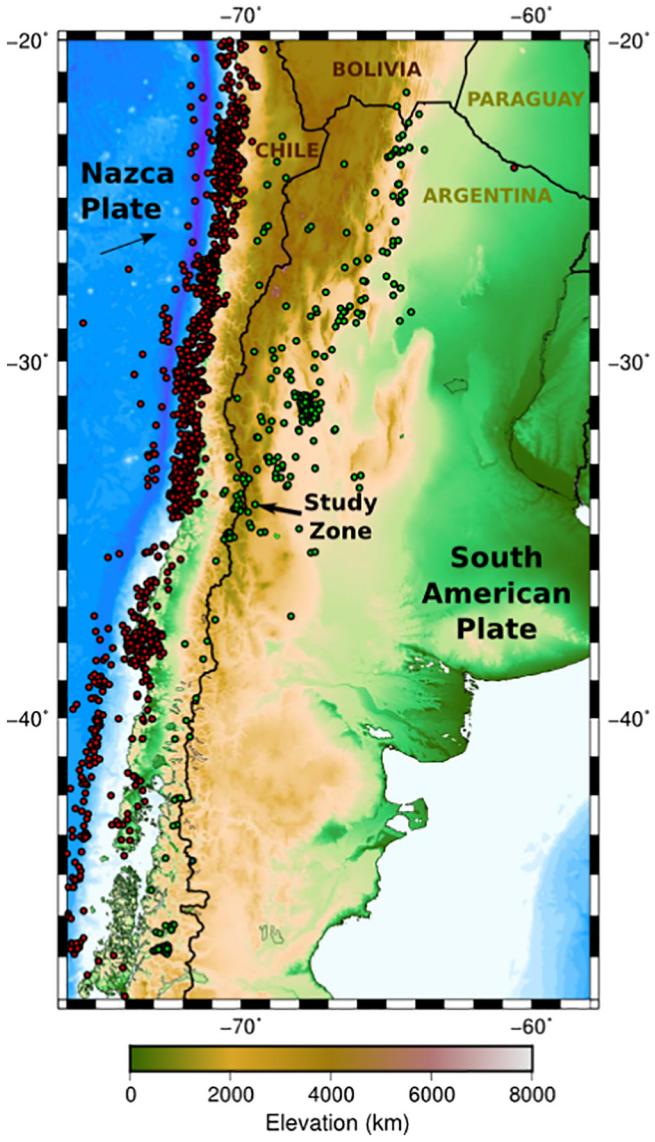


Fig. 1. Seismicity (depth: 0–50 km) corresponding to a period of time of ~48 years (International Seismological Centre, EHB Bulletin, http://www.isc.ac.uk, Internatl. Seis. Cent., Thatcham, United Kingdom, 2009). The EHB is a groomed version of the ISC Bulletin, and contains data for 141,478 events from 1960 to 2008. The Engdahl et al. (1998; EHB) algorithm has been used to significantly improve routine hypocenter determinations made by the ISS, ISC and PDE. The epicenters located between the trench and the coastal zone correspond to the interplate seismicity (red circles) associated with the contact between the Nazca and South American plates. The epicenters located partly in the fore-arc, and basically at the intra-arc and back-arc zones correspond to the intraplate seismicity (red circles) associated with the South American plate and in particular to mountain building processes. Note the strong change in the pattern of seismicity from an active back-arc in the north to an active fore-arc and intra-arc south of ~34°S. (For interpretation of the references to colour in this figure legend, the reader is referred to the web version of this article.)

Crustal earthquakes through these latitudes have been registered by global (Fig. 1) and by regional/local networks (Alvarado, 1998; Pardo et al., 2002; Barrientos et al., 2004; Farías, 2007) showing this transition in the pattern of seismicity at around 34°S. Barrientos et al. (2004) studied this seismicity at the transition area, locating it no deeper than 20 km and close to the Chile-Argentina boundary. Thus, this shallow crustal seismicity has become aligned with a structure that conforms The El Fierro Fault (Farías, 2007).

This work provides precise location of these very shallow earthquakes through the transition zone between an active back-arc in the north through the Southern Central Andes and an active fore-arc and intra-arc in the south and focal mechanism solutions from a dense network (Fig. 2). To obtain well-resolvable hypocenter determinations we used a location technique to relocate seismicity that tests the entire solution space by a direct and grid search method (Rodi, 2006). The location parameters of a set of events are determined jointly with travel-time corrections associated with the paths between the recording stations and the seismic events. As mentioned, at the latitudes of the study zone (Fig. 1), crustal earthquakes experiment a drastic change from the retro-arc north of ~34°S to the intra-arc and fore-arc zones south of this latitude. This change coincides with a strong variation in the patterns of rainfall and erosion. While north of these latitudes the fore-arc is essentially dry, south of these latitudes Pacific-derived winds provoke a drastic increment in rain fall.

Analogue and numerical experiments suggest that climate and erosion (e.g. storm runoff), play a crucial role controlling patterns of tectonic deformation and metamorphism across orogens, determining uplift and exhumation rates (e.g. Persson and Sokoutis, 2002; Dadson et al., 2003). This work, allow discussing the potential of climate and erosion in focusing crustal deformation through new data collected from a local network at one of the most striking sites of crustal seismic segmentation along the Southern Central Andes. Thus a connection is proposed between the development of fore-arc and intra-arc seismicity south of 34°S, a noticeable fall of this activity in the retro-arc zone and rainfall and short- and long-term erosion rates established in previous works.

Additionally, a discontinuous pattern in fore-arc and intra-arc crustal seismicity is observed south of 34°S at the Southern Central Andes. This pattern is discussed on the light of variable elastic thicknesses and thermal structure of the fore- and retro-arc zones. Thus, gravity data are used to calculate elastic thicknesses through the continent that are compared with earthquake density through the fore-arc identifying zones where low crustal rigidity could be inhibiting seismic activity.

1.1. Seismotectonic and tectonic settings

Seismicity shows that western South America is characterized by a convergent margin, in which the Nazca, Cocos and Antarctica plates are subducted underneath the South American plate with variable angles that range between ~30° and 0° (Cahill and Isacks, 1992; Pardo et al., 2002; Anderson et al., 2007; Nacif et al., 2015). In particular, the Nazca plate subducts at a rate of 6.7 ± 0.2 cm/yr constrained by GPS measurements along the Chile-Peru oceanic trench (Kendrick et al., 2003). Along the convergent margin between the Nazca and South American plates, changes in the angle of subduction can be either abrupt or transitional such as in the Southern Central Andes (Fig. 1), where the Nazca plate progressively steepens from a flat geometry north of ~33°S to a "normal" (~30°E) geometry south of this latitude (Cahill and Isacks, 1992; Araujo and Suarez, 1994; Pardo et al., 2002; Syracuse and Abers, 2006; Anderson et al., 2007; Nacif et al., 2015), associated with the development of an active volcanic arc (Hildreth and Moorbath, 1988; Kay et al., 2005). This active volcanism comprises the northern part of the Andean Southern Volcanic Zone, absent to the north from ~9–10 My through the Chilean-Pampean flat subduction zone (e.g., Kay et al., 1987). Additionally, the Andean margin through these latitudes is characterized by an along strike curvature known as the Maipo Orocline developed during the Neogene, interpreted as the product of a shortening gradient (Yáñez et al., 2002; Farías et al., 2008). South of these latitudes a complex pattern of mantle upwellings characterizes the retro-arc zone associated with intra-plate volcanism. While part of this dynamics is related to mantle-plume activity feeding the Payenia volcanic plateau developed between 35° and 37°S (Burd et al., 2014), a

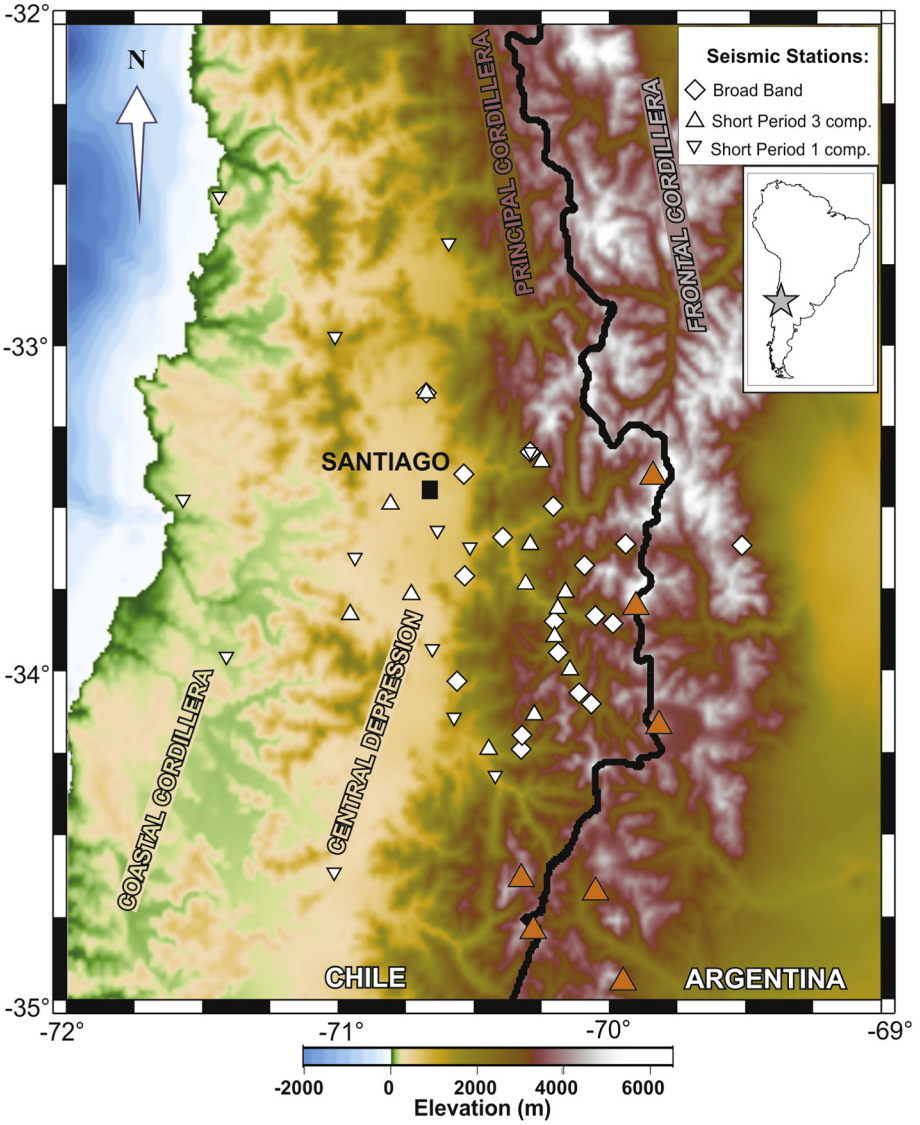


Fig. 2. Study region with stations corresponding to the CHASE Experiment. Most of the stations are located in Principal Cordillera while others lie in the Central Depression and Coastal Cordillera with only one in the eastern Andean slope in the Frontal Cordillera in Argentina. Active volcanoes are shown by orange triangles (Hildreth and Moorbath, 1988.). The upper inset shows (gray star) the study region in South America as a reference.

southern anomaly is most likely related to a slab tearing that affected the subducted Nazca plate at ~38°S feeding the Auca Mahuida and Colorado volcanic plateaux (Pesicek et al., 2012).

At the transition zone between the flat to the steeper subduction zone (~33°S to 36°S), five morphostructural units comprise the Andes, which are, from west to east (Figs. 2 and 3): a Coastal Cordillera, a Central Depression, the Principal Cordillera, the Frontal Cordillera and a back-arc (foreland) region characterized by the uplift of isolated basement blocks such as the San Rafael Block. Contrasting decollement depths characterize these systems as well as different timings of uplift determined by surficial geology and synorogenic sedimentation. The Coastal Cordillera constitutes the remnants of a Neopaleozoic accretionary prism with a Cretaceous to Neogene exhumation separated from the Principal Cordillera through the Central Depression (Hervé et al., 1988, 1994). The Principal Cordillera constitutes the drainage divide area associated with the inversion of a Mesozoic rift system linked to the Neuquén Basin (Giambiagi et al., 2009). This system experienced an extensional reactivation in Eocene to early Miocene times producing intra-arc depocenters that hosted the Abanico Fm. (see Farías, 2007; Mpodozis and Cornejo, 2012 for recent syntheses). These normal faults are inverted at the time of arc expansion that started in late early Miocene times represented by the Farellones Fm. emplaced on both sides of the Principal Cordillera. To the east, the Frontal Cordillera is part of a wide broken foreland system linked to the development of the Chilean-Pampean flat subduction zone associated with deep decollements that expose Paleozoic rocks over synorogenic Neogene strata (see Ramos et al., 2002, for a synthesis).

As depicted in Fig. 1, the eastern topographic break of the Principal Cordillera north of ~34°S is where most of the seismic activity occurs, changing this pattern towards the axial and western slope of the Andes south of this latitude. This transition zone has been affected by two relatively large (>6.0) shallow earthquakes: the Mw 6.3, September 4th 1958, "Las Melosas" earthquake (Alvarado et al., 2009) and the Mw 6.5, August 28th 2004, earthquake (Harvard CMT). Alvarado et al. (2009), using body-wave modeling estimated fault orientation, a focal

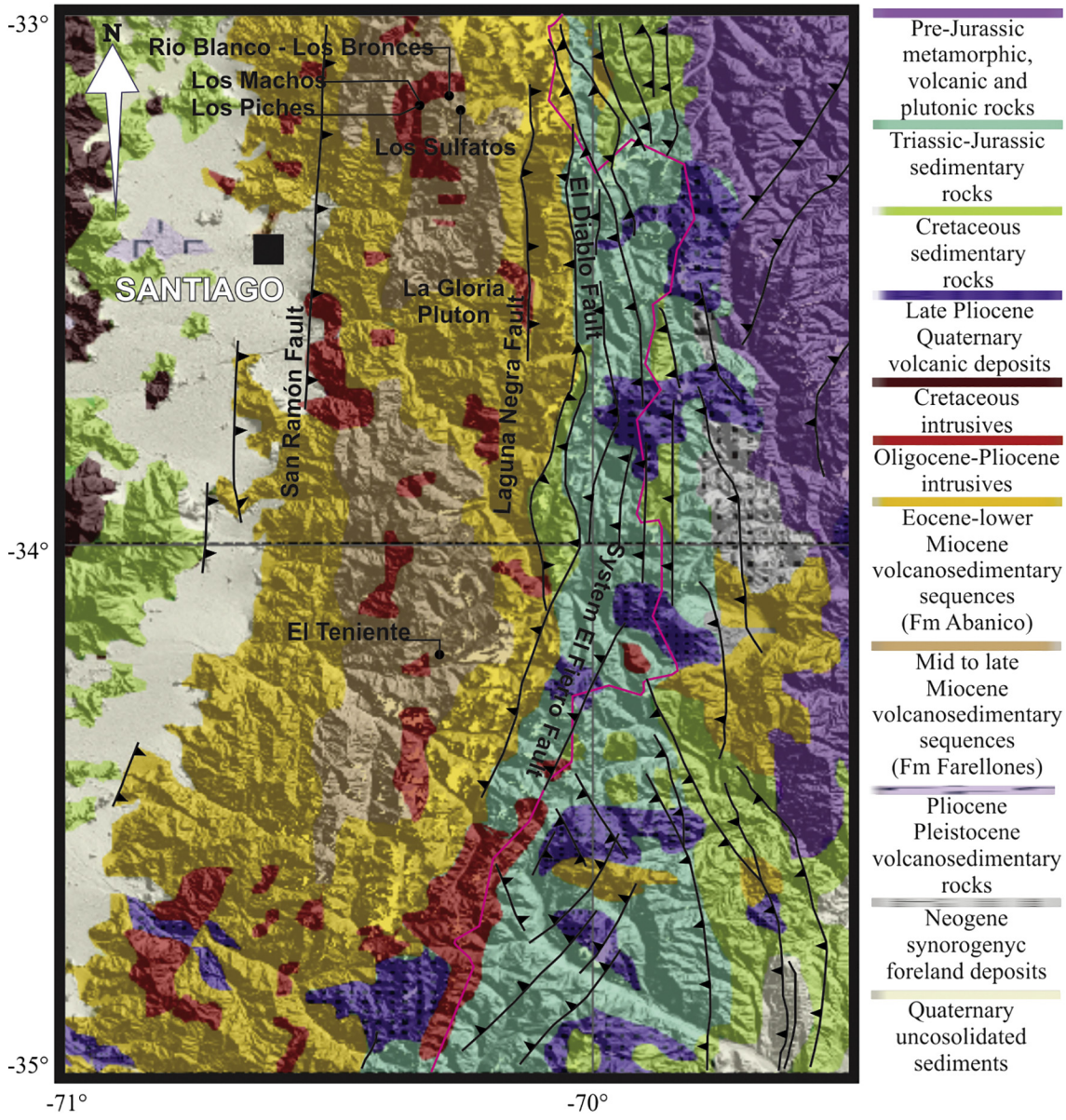


Fig. 3. Geological map of the study area from the western slope of the Andes where outcrops of the Abanico and Farellones formations are deformed in a west-vergent system to the eastern slope characterized by an eastward vergence deforming Mesozoic and Paleozoic rocks in the Aconcagua and Malargüe fold and thrust belts (data compiled from Farías, 2007, Mpodozis and Cornejo, 2014, and works cited therein). Also different mines are located here.

depth of 8 km and a size of Mw 6.3 for the 1958, "Las Melosas" earthquake. They found a focal mechanism solution with nodal planes on an east-west and north-south direction associated with right-lateral and left-lateral displacements, respectively. Their preliminary interpretation favored an activation of east-west structures, which could be accommodating latitudinal gradients in shortening north and south of ~33°S, in accordance with shortening gradients proposed for the Maipo Orocline. Contrastingly, the Mw 6.5 earthquake on August 28th 2004, located at a depth of 16 km (depth constrained from Harvard CMT) with an aftershock sequence recorded by a local network in Chile had a focal mechanism solution resolved by Harvart CMT (Centroid Moment Tensor) with one nodal plane oriented in NNE-SSW direction (with dextral strike-slip component) which is consistent with the aftershocks distribution. Another strike slip solution (Mw 6.0 on June 7th 2012), similar to 2004 earthquake, is published by CMT Catalog to the south of 36°S. However, thrust solutions are also resolved by Harvard CMT.

2. Data and methods

2.1. Seismic experiment and earthquake processing

The Chile Argentina Seismic Experiment (CHASE) was conducted in Central Chile and registered since November 2005 to March 2006 (Fig. 2). The array consisted in broad band and short period 3 components and 1 vertical component seismometers using different acquisition systems. The different format data were converted to SEISAN format (Havskov et al., 2007) and a visual inspection was performed to find seismic events using SEISAN multitrace. After continuous registers were visualized, we created an event database, maximizing the number of seismic

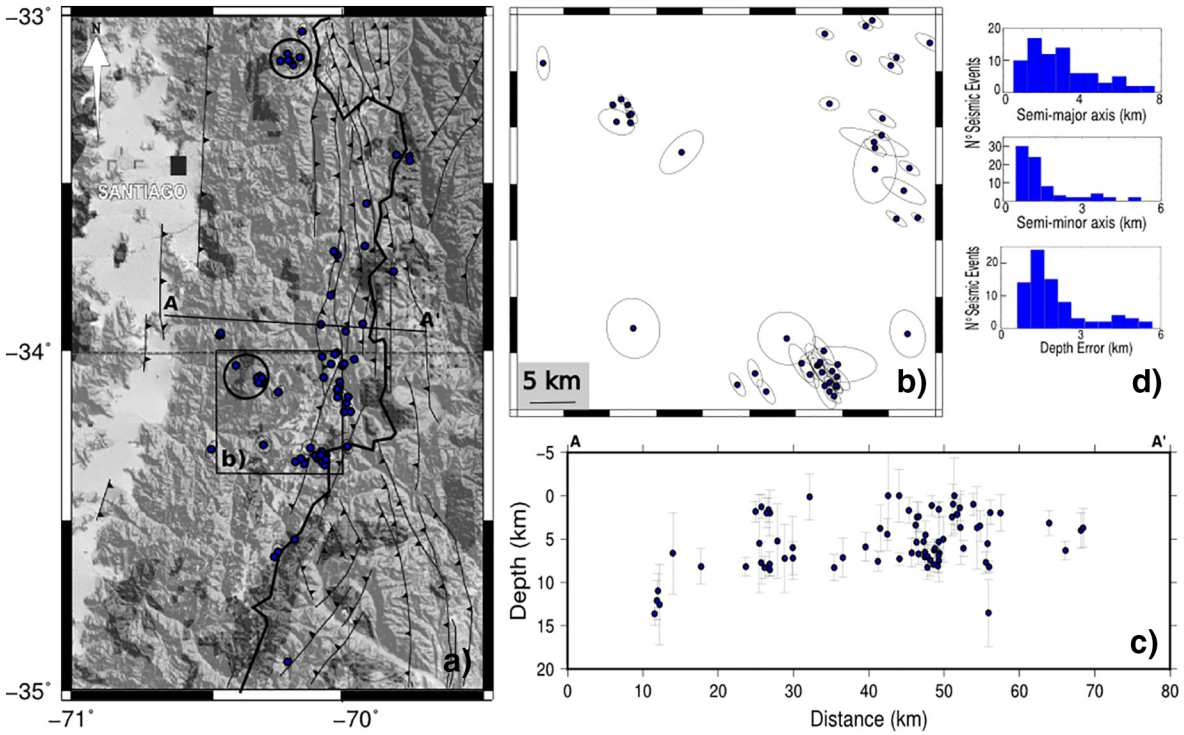


Fig. 4. Final results (from GMEL) selected after different quality tests, with their respective errors. a) Epicenters (blue circles) with their horizontal errors (black ellipses). In most cases the error is smaller than the size of the epicenter (blue circle). The two black circles enclose epicenters that could be related to triggered seismicity associated with the mining activity (see Fig. 3). The square in a) shows the region plotted in b). b) Epicenters and their horizontal errors in an amplified view. c) Cross section shows the hypocenters (blue circles) projected in A-A´ profile with their depth error (black bars). d) Histograms with horizontal (semi-major and minor axis of error ellipse) and vertical errors. (For interpretation of the references to colour in this figure legend, the reader is referred to the web version of this article.)

events which were found. P and S wave arrival identification was made using SEISAN multitrace view and coda magnitude was determined in vertical channel. In this work we only report seismic events detected at the overriding South American plate.

The location process was conducted in two stages, using HYPOCENTER (Liener and Havskov, 1995) and GMEL (Rodi, 2006) which are a single event location code and a multiple event location code, respectively. The one dimensional velocity model used in this work is from Nacif et al. (2015). To remove systematic errors related to arrival time data due to incorrect station parameters (location or timing) and/or low quality arrival times due to low signal/noise level, we based on Maurer et al. (2010). The relocation process was made using GMEL (Rodi, 2006) after a selection of a subset from HYPOCENTER results. GMEL applies a maximum-likelihood grid search algorithm to find location parameters within a cluster of events and solves station travel-time correction simultaneously. Thus, a grid-search algorithm was applied that constitutes a method that allows the association of a set of arrivals to a particular event. Using TauP Toolkit (Crotwell and Owens, 1998) we calculated the travel time tables (step of 1 km and 0.01° for depth and epicentral distance) using the velocity model from Nacif et al. (2015) from which the theoretical times were extracted. Errors in the arrival identification phases (picking errors) are basically random in character. GMEL considers that these errors have approximately a Gaussian (or power exponential) probability distribution (Rodi, 2006).

Two methods for determining earthquake focal mechanism from first P motion polarities, FOCMEC (Snoke et al., 1984) and HASH (Hardebeck and Shearer, 2002) were used. FOCMEC code performs and optimizes systematic search of the focal sphere and reports acceptable solutions based on selection criteria for the number of polarity errors. HASH finds a set of focal mechanisms for each event that are acceptable, given the P-wave polarities at a set of stations, the azimuth, the takeoff angle to each station and estimation of uncertainty in those input parameters to test the stability of the focal mechanism solutions. The preferred solution is therefore found by averaging the acceptable solutions, after removing any outliers (solutions which are farthest from the average). The focal mechanism quality parameters that are computed by HASH program (Hardebeck and Shearer, 2002; Kilb and Hardebeck, 2006) are: the root-mean-square (RMS) angular difference between the set of acceptable mechanisms and the preferred mechanism (which ranges 0° to 90°), evaluation of overall fit (which ranges 0.0–1.0, with a 0.0 value representing a perfect fit to the data while 1.0 represents a perfect misfit), station distribution ratio (which ranges 0.0–1.0, with low values indicating that a relatively large number of data points lies near nodal planes in the solution), maximum azimutal gap (which ranges 0° to 360°), number of first motion observations and mechanism probability (which ranges 0.0–1.0, where a large value indicates that most of the acceptable solutions are close to the preferred mechanism). By evaluation of the last parameters, HASH achieves a quality factor which divides the solutions in 6 qualities (A, B, C, D, E and F; in which A is the best solution and F is the worst solution). This gives a good estimate about the mechanism stability which allows establishing a degree of confidence in the results.

2.2. Gravity data and elastic thickness calculation

To calculate the elastic thickness we used the convolution method approach (Braitenberg et al., 2002) that has been widely tested in different areas with different tectonic settings (Braitenberg et al., 1997; Braitenberg and Drigo, 1997; Zadro and Braitenberg, 1997; Braitenberg and Zadro, 1999; Ebbing et al., 2007; Braitenberg et al.,

Table 1
Location parameters for 77 South American intraplate seismic events after run GMEL software (Rodi, 2006) and applied different test to the data. In magnitude column the "-" means that there is no a determined magnitude and "*"means that that is local magnitude (NEIC-USGS) instead coda magnitude (only for four earthquakes) symbol m* in The location uncertainties were obtained from a confidence coefficient of 90%, which are represented in the horizontal (in which the strike angle refers to the azimuth of s_{max} axis) by s_{max} (semi-major axis), s_{min} (semi-minor axis) and in the vertical by ± edepth (error in depth). The residual in time is evaluated by Time Weighed Residual Norm (TWRN). The results were calculated considering that data errors obey to a Laplace distribution or two-sided exponential.

Seismic events parameters						Location uncertainties parameters			
Origin Time	Location parameters			Magnitude	TWRN	Error ellipse			edepth
Year/Month/Day/Hour/Min./Sec.	Long. (°)	Lat. (°)	Depth (km)	(Coda)	(*sec*)	Strike (°)	s_{majax} (km)	s_{minax} (km)	(km)
2005/12/01/02/06/47	−69.9689	−33.688	1.96	2.1	0.174	59.87	3.15	1.19	1.39
2005/12/05/12/08/15	−70.1052	−34.3097	5.33	1.5	0.057	271.64	7.68	3.54	4.56
2005/12/16/11/04/06	−69.8134	−33.4219	4	1.5	0.294	47.39	3.41	1.83	2.06
2005/12/17/22/05/42	−70.1138	−34.079	5.36	0.5	0.126	276.84	2.04	1.28	1.56
2005/12/22/03/06/24	−70.0888	−33.8349	2.47	0	0.066	59.39	1.05	0.87	1.75
2005/12/28/02/16/31	−70.2399	−34.9163	0	1.5	0.262	359.11	4.7	2.37	5.22
2006/01/04/18/52/49	−70.3384	−34.0746	1.29	1.1	0.138	339.78	0.97	0.59	1.38
2006/01/05/21/24/46	−70.2652	−33.1359	8.19	2.5	0.287	47.25	1.16	0.71	1.09
2006/01/06/09/25/45	−70.0658	−33.7146	7.07	1.6	0.308	81.6	0.73	0.56	0.61
2006/01/07/16/36/31	−70.0742	−33.7068	2.41	1.2	0.099	36.81	1.75	1.1	1.64
2006/01/07/23/15/19	−70.0784	−33.7037	3.4	–	0.086	25.51	2.73	1.41	1.5
2006/01/08/01/47/12	−70.1354	−34.3185	6.73	0.7	0.364	328.72	2.94	1.19	1.19
2006/01/08/03/08/24	−70.1062	−34.3299	6.62	3.0*	0.427	323.26	1.54	0.74	0.84
2006/01/08/03/46/27	−70.1142	−34.3261	7.94	2.5*	0.382	322.63	1.5	0.76	0.82
2006/01/08/07/31/53	−70.1139	−34.3335	6.29	1.7	0.355	337.03	2.06	0.93	1.03
2006/01/08/08/24/23	−70.1068	−34.329	6.91	2.5*	0.341	316.67	1.8	0.8	0.88
2006/01/08/08/51/34	−70.1107	−34.3158	6.09	–	0.412	328.2	2.79	1.1	1.1
2006/01/08/10/06/04	−70.1217	−34.317	8.26	–	0.369	323.46	3.46	1.2	1.35
2006/01/08/10/23/43	−70.1444	−34.309	6.6	1.5	0.115	330.41	4.3	1.59	1.65
2006/01/08/10/31/28	−70.1604	−34.2873	0	–	0.121	291.36	5.71	5.11	3.09
2006/01/08/23/15/17	−70.1269	−34.3113	5.3	1.4	0.352	327.22	3.02	0.99	1.13
2006/01/09/03/16/12	−70.4221	−34.0428	8.18	–	0.013	355.88	3.33	1.27	2.04
2006/01/09/03/45/43	−70.1189	−34.3288	7.44	2.2	0.066	340.26	4.76	1.76	1.79
2006/01/09/08/24/26	−70.109	−34.3379	8.11	2.8*	0.327	316.84	1.84	0.81	0.82
2006/01/10/03/54/20	−70.1249	−34.3105	6.54	1.8	0.194	329.2	4.67	1.59	2.11
2006/01/10/03/58/48	−70.0302	−34.2827	13.52	1	0.107	345.08	4.73	3.37	3.89
2006/01/10/17/00/27	−70.2414	−33.1149	7.73	2	0.087	14.86	4.57	3.49	2.42
2006/01/18/11/56/49	−70.4797	−33.9537	13.63	1.8	0.183	347.41	0.52	0.51	1.36
2006/01/19/01/04/34	−70.3283	−34.0961	8.55	1.5	0.144	313.61	0.8	0.48	0.74
2006/01/19/03/27/08	−70.5077	−34.2909	12.56	2.2	0.018	27.1	6.3	2.75	4.68
2006/01/19/07/10/57	−70.1055	−34.3208	7.49	1.8	0.069	315.86	3.48	1.31	1.37
2006/01/21/11/13/08	−70.0189	−34.1799	8.21	1.5	0.232	305.4	1.39	0.63	0.69
2006/01/22/01/23/30	−69.868	−33.7644	6.33	–	0.104	337.89	1.39	0.85	1.09
2006/01/26/17/32/57	−70.1196	−34.2976	7.04	1.3	0.092	325.17	3.37	1.1	1.59
2006/01/29/18/37/49	−70.0567	−34.0919	2.17	2	0.024	300.98	3.08	0.98	1.78
2006/02/01/02/11/01	−70.1238	−34.3084	4.54	0.8	0.145	324.35	2.46	0.87	1.58
2006/02/01/13/23/34	−70.475	−33.9529	10.98	1.1	0.163	353.58	1.06	0.85	1.97
2006/02/03/22/23/43	−70.1822	−34.3341	4.45	2	0.177	326.4	2.79	1.06	1.85
2006/02/07/23/12/14	−70.0885	−34.0388	1.13	–	0.071	310.64	1.77	1.15	1.18
2006/02/09/22/15/51	−69.8583	−33.4172	3.16	1.3	0.217	55.95	2.54	1.28	1.41
2006/02/10/22/28/48	−70.221	−33.1476	5.24	1.6	0.08	338.55	6.09	4.03	4.26
2006/02/11/16/44/53	−70.2309	−33.1359	7.9	1.8	0.144	22.19	3.23	1.32	1.4
2006/02/16/04/56/12	−70.5651	−35.0144	6.63	1.8	0.354	352.7	2.7	1.47	4.71
2006/02/16/17/13/27	−69.8105	−33.4336	3.72	2.2	0.119	59.5	4.1	1.54	2.27
2006/02/17/03/42/57	−70.0653	−34.1374	0	1.9	0.171	6.51	6.73	4.24	4.37
2006/02/18/02/16/09	−70.0282	−34.1362	3.49	1.1	0.103	301.82	2.37	0.94	1.75
2006/02/18/18/06/33	−70.2376	−33.1337	8.29	1.4	0.131	62.71	1.6	0.92	1.26
2006/02/19/13/45/56	−70.2726	−34.5943	7.15	–	0.054	347.53	5.97	3.35	2.27
2006/02/21/10/01/10	−70.4758	−33.9472	12.1	0.4	0.067	352.27	1.54	0.75	2.25
2006/02/24/21/47/51	−70.1892	−33.048	7.21	2.4	0.071	12.76	5.68	3.1	1.91
2006/02/28/20/18/01	−70.2732	−34.1219	0.12	1.9	0.058	45.39	5.44	2.67	2.69
2006/03/03/19/10/37	−69.9769	−33.9201	2	0.2	0.107	274.83	1.83	0.76	2.09
2006/03/05/07/23/20	−70.3248	−34.2781	7.24	2.3	0.006	347.94	5.92	5.24	3.94
2006/03/05/12/47/34	−70.0676	−34.0048	5.04	1.5	0.015	299.33	2.36	1.07	2.62
2006/03/09/07/29/57	−70.0745	−34.0095	1.57	1.4	0.143	292	1.48	0.72	0.9
2006/03/10/09/00/50	−70.3295	−34.0886	1.63	1.4	0.078	328.66	1.02	0.64	1.39
2006/03/10/09/25/08	−70.0339	−34.1564	3.7	1.5	0.087	298.87	4.82	1.57	4.72
2006/03/11/05/48/55	−70.2154	−34.5574	3.78	1.9	0.171	351.68	3.86	2.31	2.7
2006/03/12/09/00/51	−70.1941	−34.3176	7.57	1.5	0.202	339.73	2.89	1.14	1.16
2006/03/12/20/30/20	−70.3467	−34.08	1.82	1.6	0.166	327.82	0.83	0.56	1.21
2006/03/13/05/10/21	−70.0365	−33.9419	3.67	1.9	0.034	302.81	2.41	1.35	4.24
2006/03/14/04/55/50	−70.3267	−34.0877	2	1.9	0.228	332	2.13	0.8	2.61
2006/03/14/06/00/55	−70.0476	−34.0446	1.39	0.8	0.034	302.04	2.67	1.05	1.49
2006/03/16/09/10/18	−70.3313	−34.0796	2	1.9	0.136	339.23	1.38	0.63	1.75
2006/03/18/23/47/07	−70.0419	−34.1812	0.99	1.8	0.162	306.64	2.49	0.71	1.3
2006/03/19/00/10/44	−70.2866	−34.6076	8.31	1.1	0.487	322.06	2.49	1.14	1.53
2006/03/19/09/14/40	−70.0416	−34.0384	6.07	1.4	0.162	292.7	1.67	0.7	0.96

(continued on next page)

Table 1 (*continued*)

Seismic events parameters						Location uncertainties parameters			
Origin Time	Location parameters			Magnitude	TWRN	Error ellipse			edepth
Year/Month/Day/Hour/Min./Sec.	Long. (°)	Lat. (°)	Depth (km)	(Coda)	(*sec*)	Strike (°)	s_{majax} (km)	s_{minax} (km)	(km)
2006/03/19/09/41/36	−70.0056	−34.0249	5.53	0.6	0.127	299.81	3.25	1.17	3.24
2006/03/19/17/49/00	−70.0576	−34.1066	2.14	1.2	0.215	299.62	1.81	0.73	1.34
2006/03/19/18/16/06	−70.1972	−33.1257	6	2	0.221	350.26	4.95	2.94	3.65
2006/03/21/02/27/58	−70.0649	−34.1183	0.98	1.9	0.053	304.49	2.61	0.94	2.36
2006/03/22/03/16/08	−70.0656	−34.1133	2.45	1.8	0.012	288.81	7.2	1.71	2.19
2006/03/22/06/25/18	−69.9629	−33.5624	7.7	2.1	0.106	69.22	1.69	0.84	1.24
2006/03/22/15/28/21	−70.1188	−34.0169	1.7	2.4	0.036	290.12	1.81	0.98	1.5
2006/03/27/02/19/25	−70.1229	−33.9216	7.29	1	0.322	278.78	1.1	0.63	0.72
2006/03/27/04/31/31	−70.343	−34.0949	5.5	2.5	0.041	293.45	3.7	2.28	5.68
2006/03/28/00/15/53	−70.2128	−34.3283	5.91	1.7	0.256	328.92	2.62	0.98	1.65

2002; Wienecke et al., 2007; Gimenez et al., 2009; Alvarez et al., 2015a, 2015b). This method involves the solution of the fourth order differential equation that describes the flexion of a thin plate (a concept introduced by Vening-Meinesz, 1939). This procedure allows the analytical calculation of the deflection of a plate with an irregular topographic load (Wienecke, 2006). Additionally, it calculates the flexural parameters between the crust-mantle interface obtained by gravity inversion (observed Moho) and the crust-mantle interface provoked by the deflection of the topographic load (flexure model). In order to calculate the elastic thickness (Te) the Lithoflex software was used (Braitenberg et al., 2007; Wienecke et al., 2007). To calculate the crust-mantle discontinuity produced by the topographic load, we used the digital elevation model ETOPO1 (Amante and Eakins, 2008). From the gravity model EGM2008, up to degree and order 2159 (Pavlis et al., 2008, 2012), we estimated the undulation of the gravimetric discontinuity between the crust and upper mantle by gravimetric inversion. This method is based on an iterative algorithm that alternates downward continuation with direct forward modeling (Braitenberg and Zadro, 1999) and is somewhat analogous to the Oldenburg – Parker inversion approach (Parker, 1972; Oldenburg, 1974; Braitenberg et al., 2007).

Calculation of the elastic thickness requires as input parameters density contrast and mean reference depth. The contrast between the crust and the upper mantle was assumed as a constant value of −0.4 g/cm3 and for the normal crust thickness the standard value used is 35 km. The densities adopted are standard values previously used by Introcaso et al. (2000), Gimenez et al. (2000) and Miranda and Robles (2002) for nearby regions. The range of values in which the elastic thickness varies must be limited. For this study we considered a range between $1 < Te < 50$ km, in moving windows of 40 km × 40 km for the study area. In order to avoid border effects, the area of analysis was extended 20 km away from the study area.

3. Results

3.1. Seismic experiment and earthquake processing results

Before obtaining the final results (Fig. 4 and Table 1), we chose a subset of events for the relocation process with the most constraining results and lowest weighted residual norm (wrn). The selection criterion was semi-major axis of error ellipse <20 km (horizontal error), semi-confidence interval < 20 km (vertical error) and

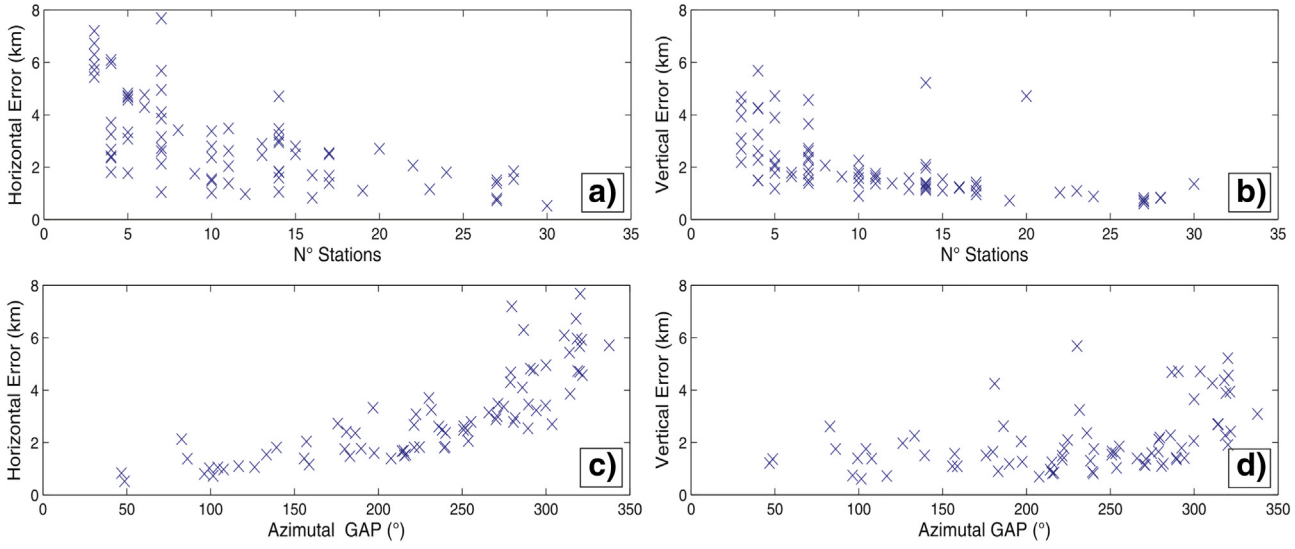


Fig. 5. Depth error analysis for the 77 earthquakes which are shown in Fig. 4 and Table 1. Blue crosses constitute the different earthquakes. The horizontal a) and b) vertical errors are plotted against the numbers of stations used for each earthquake location. The horizontal c) and d) vertical errors are plotted against the azimutal GAP. (For interpretation of the references to colour in this figure legend, the reader is referred to the web version of this article.)

Table 2
Preliminar focal mechanism solutions obtained from P first motion using HASH software. Equal area projection of inferior hemisphere was used. IN: Identification Number. The two nodal planes are indicated by $strike_N$, dip_N and $rake_N$ parameters. The solutions that are shown in this work (strike, dip and rake of each nodal plane) represent a preferred solution which was obtained by the HASH after a set of acceptable solutions for each event were averaged. The uncertainties in the strike and dip (nodal plane 1) are given by $strike_{NP1}$ and dip_{NP1}, respectively. The quality (Qual.) criterion is from Hash et al. 2005. The percent of real mechanisms "close" to average mechanism is given by PMNS.

IN	Seismic events parameters				Focal mechanism solutions										
	Origin Time	Long.	Lat.	Depth	Nodal plane 1 (°)			Nodal plane 2 (°)			Uncertainties (°)		N°	Qual.	PMNS
	Year/Month/Day/Hour	(°)	(°)	(km)	Strike	Dip	Rake	Strike	Dip	Rake	$Strike_{np1}$	Dip_{np1}	Pol		
1	2006/01/06/09/25/47	−70,0658	−33,7147	7,07	103	35	29	349	74	121	26	29	23	B	69
2	2006/01/08/03/08/25	−70,1062	−34,3298	6,62	113	41	−40	235	65	−123	42	42	26	D	33
3	2006/01/08/03/46/28	−70,1142	−34,3262	7,94	43	48	−120	264	50	−61	47	45	21	D	26
4	2006/01/08/08/24/24	−70,1068	−34,329	6,91	35	41	−107	237	51	76	43	41	20	D	32
5	2006/01/18/11/56/51	−70,4797	−33,9537	13,63	190	72	87	20	18	99	33	34	21	B	60
6	2006/01/19/01/04/35	−70,3283	−34,0962	8,55	264	18	−38	31	79	−104	48	57	16	D	23
7	2006/01/21/11/13/10	−70,0188	−34,1798	8,21	46	65	−147	301	60	−29	49	45	17	D	25
8	2006/02/01/13/23/36	−70,475	−33,9528	10,98	195	87	125	289	35	5	50	55	10	D	22
9	2006/02/21/10/01/12	−70,4758	−33,9472	12,1	151	81	86	355	10	114	49	50	10	D	22
10	2006/03/19/09/14/40	−70,0417	−34,0383	6,07	11	76	−172	279	82	−14	49	51	14	D	26
11	2006/03/19/17/49/01	−70,0577	−34,1067	2,14	7	52	−103	208	40	−74	46	43	12	D	31

wrn < 0.5 s. From these relocated earthquakes, 12 seismic events which presented horizontal and/or vertical errors higher than ±8 km were rejected. When the number of stations became higher than 8, horizontal and vertical errors decreased noticeably (Fig. 5a and b). The best results according to the weighted residual norm were obtained considering that data errors follow the Laplace distribution (two-sided exponential). Otherwise higher errors appeared when the azimuthal gap was >275° (Fig. 5c and d). The final results showed 77 intraplate events with less scattered solutions that located mainly in the first 10 km of the upper crust. The magnitudes of these earthquakes go from 0.2 to 3.0.

The HASH quality indicator found only 2 with good quality for the 11 solutions (for details see quality table in Hardebeck and Shearer, 2005). The focal mechanisms with quality D exhibit large uncertainties in nodal plane determinations and low probability to find the real mechanism near the solution. Otherwise events 2, 3 and 4 (Table 2) with quality D correspond to a set of main shock and their aftershocks. So considering that the azimuthal distribution of the first motions is not enough to construct a single focal mechanism for these three earthquakes, we computed the composite focal mechanisms solution (67 P-wave polarities data) achieving a more reliable solution (Sbar et al., 1972). In order to solve the composite focal mechanism one major assumption is taken in which the used aftershocks need to share the same focal mechanism (the same radiation pattern) as the main shock. We run HASH code in SEISAN platform to find the composite focal mechanism solution for these three events and consequently the uncertainties in nodal plane determination notably diminished. Table 3 and Fig. 6 show the final focal mechanism solutions.

3.2. Elastic thickness results and relation to crustal seismicity

When interpreting the computed Te values, representative of crustal rigidity, these highlight the increase of rigidity in the back-arc over the flat-slab region, as noted in previous works (Stewart and Watts, 1997; Tassara, 2005; Alvarez et al., 2015a). Perez-Gussinyé et al. (2008) proposed that flat slabs are characterized by high Te values, high shear wave velocity, thick thermal lithosphere and low heat flow. In this setting, the subducted slab flattens, traveling subhorizontally and repelling the asthenospheric wedge hundreds of kilometers to the east. Intraplate seismicity (Fig. 7) is well correlated with high Te values in the back-arc region over the flat slab, this high Te value is explained by the absence of a magmatic arc since the Late Miocene. Similar results were found by Alvarez et al. (2015a).

Alvarez et al. (2015b) also found a close correspondence between the contours of the subducted Nazca slab (plate morphology) and Te variations (higher than 5 km) along the southern region of the flat slab. Low Te values along the Main Andean axis indicate that the plate has no strength (classical Airy model for local compensation). Te results are consistent with previous isostatic analyses for the Andean region at these latitudes (Stewart and Watts, 1997; Tassara and Yáñez, 2003; Tassara et al., 2007; Perez-Gussinyé et al., 2008; Sacek and Ussami, 2009).

South of 33°S, where the oceanic plate gets progressively steeper acquiring a 'normal' dip angle, the back-arc region is characterized by broad volcanic fields associated with deep asthenospheric anomalies (Burd et al., 2014). Low Te values estimated in this area reflect a weakened upper plate in the back-arc as shown in Fig. 7, in coincidence with the low and scarce seismicity

Table 3
Final focal mechanism solutions considering that the total of solution show in Table 2 have a low percent of real mechanisms "close" to average mechanism. The solution 2 is a composite solution using the polarities data for a M_l 3.0 principal shock (2006/01/08/03/08/25) and two of their aftershocks (2006/01/08/03/46/28 and 2006/01/08/08/24/24).

IN	Seismic events parameters				Focal mechanism solutions										
	Origin Time	Long.	Lat.	Depth	Nodal Plane 1 (°)			Nodal Plane 2 (°)			Uncertainties (°)		N°	Qual.	PMNS
	Year/Month/Day/Hour	(°)	(°)	(km)	Strike	Dip	Rake	Strike	Dip	Rake	Strike	Dip	Pol		
1	2006/01/06/09/25/47	−70,0658	−33,7147	7,07	103	35	29	349	74	121	26	29	23	B	69
2	2006/01/08/03/08/25	−70,1062	−34,3298	6,62	65	23	−65	218	69	−100	18	16	67	–	–
	2006/01/08/03/46/28	−70,1142	−34,3262	7,94											
	2006/01/08/08/24/24	−70,1068	−34,329	6,91											
3	2006/01/18/11/56/51	−70,4797	−33,9537	13,63	190	72	87	20	18	99	33	34	21	B	60

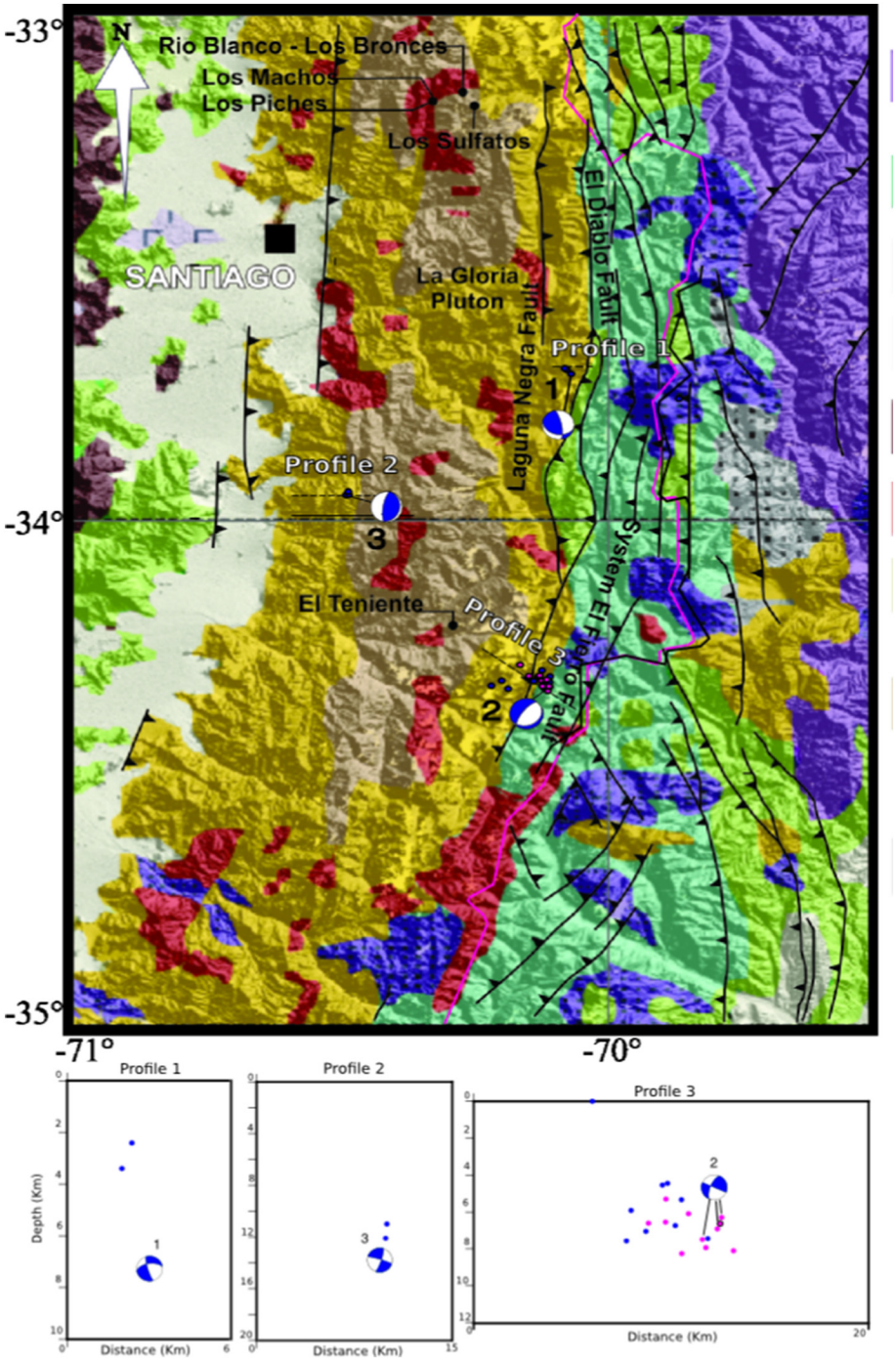


Fig. 6. Focal mechanism solutions from P-first motion using HASH code. Only epicenters near each mechanism are shown with blue circles. The southernmost mechanism is shown with the main shock (Ml = 3) and its aftershocks in violet circles. With blue colour and white colour the compressional and dilatational area are shown, respectively. Near each mechanism there is a number which correspond to the identification number in Table 3. In the three profiles there is a noticeable hypocenter alignment with one of the nodal planes. In profile 3 the seismic events used to obtain the composite solution are indicated with black line. Additionally the violet circle of the principal shock is distinguished from the other with a black line. (For interpretation of the references to colour in this figure legend, the reader is referred to the web version of this article.)

registered in this work. Along the volcanic arc (33° to 34.5°S) the cluster of shallow depth seismicity (blue circles in Fig. 7) is nucleated close to high Te values which spans along the entire fore-arc. To the south of 34.5°S shallow depth seismicity decreases as Te diminishes up to 35°S, where high Te values moves away towards the coast. South of this latitude almost all seismicity vanishes as volcanic intensity increases.

4. Discussion

Using a dense network between ~33°S to 34.5°S, and appropriate location software, we determined that most of the located crustal earthquakes appear on the western Andean slope. These data have been located with horizontal and vertical errors lesser than ±4 and ±3 km respectively, allowing assigning them to the western flank of the

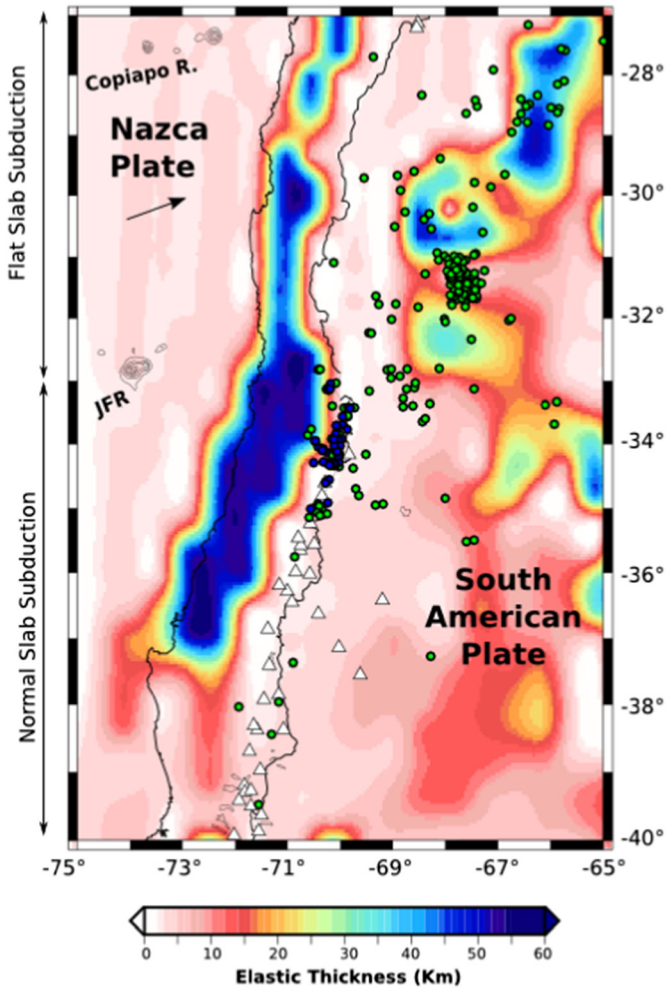


Fig. 7. Elastic thicknesses on the Andes and crustal seismicity. Note that higher earthquake density occurs at the edges of areas of relatively higher Te. North of 33.5°S crustal seismicity hosted in the back-arc nucleated in areas of high Te. Between 33.5° and 35°S seismicity concentrates in the fore-and intra-arc zones and nucleates on the edges of a rigid block associated with Paleozoic rocks outcropping in the Coastal Cordillera. Low elastic thicknesses in the transition zone from ~33°S to 39°S are explained by asthenospheric upwellings associated with slab tearing processes at ~38°S described in Pesicek et al. (2012) and plume activity between 35° and 37°S (Burd et al., 2014; see Rojas Vera et al., 2014 and Folguera et al., 2015 for a discussion). This could explain how low elastic thicknesses towards Patagonia would inhibit the development of crustal seismicity in the fore-arc and arc regions.

Principal Cordillera. Even though most of these events were located on this western flank showing an important concentration of seismic activity that is absent to the north, their number diminishes considerably to the south across the fore-arc zone. Only three reliable focal mechanisms solutions were obtained in this group (Table 3 and Fig. 6). The mechanism 1 and 3 presented thrust mechanism solutions with high and small strike-slip components, respectively. The focal mechanism 2 is obtained from a composite of three earthquakes and.

represents a normal solution with small strike-slip component. For the focal mechanism 1, we interpreted that its north-south nodal plane (although considering its dip uncertainty the dip could be smaller) corresponds to the fault plane and could be related to the activity of Laguna Negra fault described in field studies by Fock (2005). This fault was identified like a west-vergent back-thrust fault which affects Cenozoic sections (Cornejo and Mahood, 1997). So considering the focal mechanism depth, the Laguna Negra fault could be extended at deeper level. Focal mechanism 2 is interpreted as a local extensional reactivation of de El Fierro fault, which is a plausible mechanism for this sector of the Andes that has suffered since 3 Ma an extensional reactivation (Folguera and Ramos, 2009; Ramos et al., 2002). Finally, focal mechanism 3 located at a depth of ~14 km is not directly related to outcropping structures and is most likely reflecting the activity of a basal decollement. If we considered its near horizontal nodal plane (with dip uncertainty) as the fault plane, its focal mechanism could be related to the main decollement proposed by Giambiagi et al. (2014).

When plotting seismic events from southern South American from the EHB catalog with the earthquakes located in this work, a rapid change between an active back-arc north of 34°S to an almost inactive retro-arc sector in the south is seen (Fig. 8). This change coincides with a strong precipitation rate gradient through the fore-arc zone. While north of 34°S precipitation rates are below 500 mm/yr, south of these latitudes these rates rapidly increase to 700 and then above 1000 mm/yr (Fig. 9) (Carretier et al., 2014).

Besides this, there is a correspondence between the seismogenic zone implanted south of 34°S and the catchment average rates of decadal erosion from suspended sediments and millennial erosion from ^{10}Be in river sands (Fig. 9 and Fig. 10) (Pepin et al., 2010; Carretier et al., 2013, 2014). We propose as a hypothesis that precipitation and erosional rates could be determining sub-critical conditions on this region (prowedge of the subduction system in the fore- and arc-zones) triggering shallow seismicity as a need to restore the critical tape angle through out-of-sequence thrusts. Sediment trench fill south of 35°S could also play a role weakening plate coupling and hence inhibiting back-arc seismic activity.

Besides this, gradual change to higher degrees in subduction angle could also inhibit mountain building far from the Chilean trench (Nacif et al., 2015). On the fore-arc and intra-arc, crustal seismicity is almost non-existent north of 33°S implying a rigid block that is transported eastwardly at expenses of back-arc structures that accommodate shortening. Additionally, this rigid fore-arc coincides with an area of low precipitation and erosion rates. To the south, between 33.5°and 35°S, the fore-arc and intra-arc become seismically active in relation to the activity of structures in the fore-arc and intra-arc coinciding with the latitudes of higher erosion rates (Figs. 9 and 10c). Even though crustal earthquake distribution persists to the south over the back-arc sector, it develops with a marked fall in activity that could be explained by low elastic thicknesses on this region related to thermal anomalies potentially associated with asthenospheric anomalies and slab tearing processes.

(Fig. 7) (Pesicek et al., 2012; Burd et al., 2014; Sagripanti et al., 2015; Rojas Vera et al., 2014) and those processes could be affecting the fore-arc and intra-arc region. Also at the fore-arc and intra-arc region south of ~35°S there is a noticeable shallow seismicity decreases which could be associated with the increases in volcanic intensity and reflected by the moves away towards the coast of the high Te values.

5. Conclusions

From a high density-seismic network installed between ~33°S to 34.5°S over the Chilean fore-arc and axial Andean sector, the recorded shallow seismic activity is located mainly at depths shallower than 10 km on the western Principal Cordillera. This implies a strong segmentation of crustal seismicity in the Southern Central Andes from a seismically active eastern topographic break, from the Subandean system bordering the Altiplano to the Precordillera in the Chilean-Pampean flat slab to the fore-arc and intra-arc south of 34°S. Additionally, a nearly inactive back-arc at these latitudes coincides with the establishment of seismic activity on the fore-arc and intra-arc region.

This seismically active westward verging system coincides with a change in precipitation and erosion rates across the Andes as

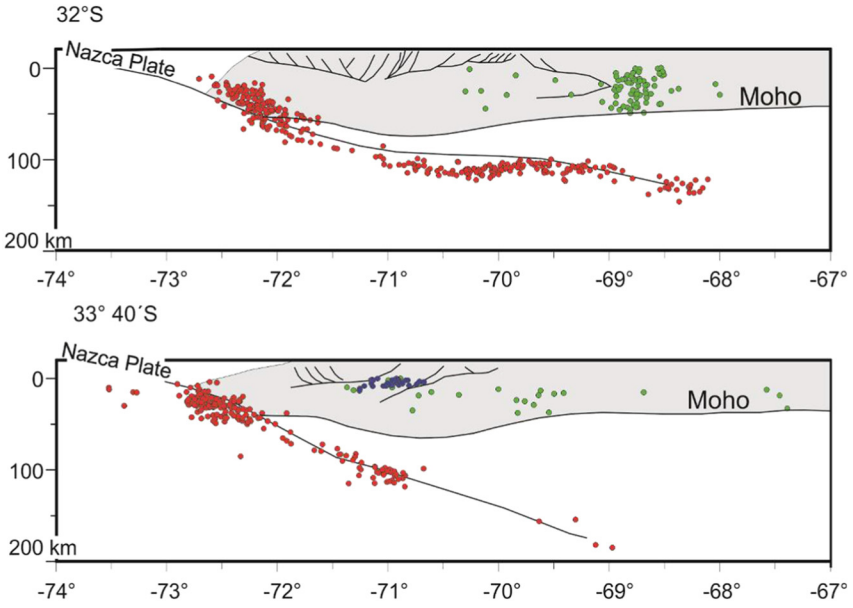


Fig. 8. Two cross sections throughout the southern Central Andes, one at the Pampean-Chilean flat subduction zone and the other over the 27°E dipping subduction zone to the south, showing structures associated with crustal seismicity and others with Neogene activity. Moho inverted from gravity data is indicated as a reference. The hypocenters from EHB Bulletin Catalog are shown with red circles (interplate seismic events) and with green circles (South American intraplate seismic events). The hypocenters located in this work are shown with blue circles. (For interpretation of the references to colour in this figure legend, the reader is referred to the web version of this article.)

determined in previous studies. This relation could be explained by subcritical states of the orogenic wedge south of 34°S. Decoupling of the subduction interface due to a thicker trench-sediment infill could also play a role inhibiting back-arc activity. However, this cannot explain the lack of seismicity in the fore-arc and intra-arc zone north of these latitudes where the trench is nearly starving. Inhomogeneous distribution of seismic activity through the fore-arc and intra-arc south of 34°S is explained by the volcanic intensity increases (along the intra-arc south of ~35°S) and by mantle anomalies associated with shallow plume activity and tearings on the Nazca plate feeding the Payenia volcanic field inferred from computed elastic thicknesses.

Acknowledgements

This material is based on work supported by **CH**ile **A**rgentina **S**eismic **E**xperiment developed by the project *"Crustal seismicity and velocity structure in the principal cordillera of central Chile 33°-34.5°S: implications on andean geodynamic and seismic hazard"*, FONDECYT 1050758, Chile, Director: Dr. Mario Pardo. Many thanks to William Rodi for allowing us to use his grid multiple events location code GMEL and assistance in using it. The authors would like to thank the CONICET (Consejo Nacional de Investigaciones Científicas y Técnicas) for financial support. The authors acknowledge to Dr. Mario Pardo, Dra. Patricia Alvarado and Dr. Sergio Barrientos for their useful comments.

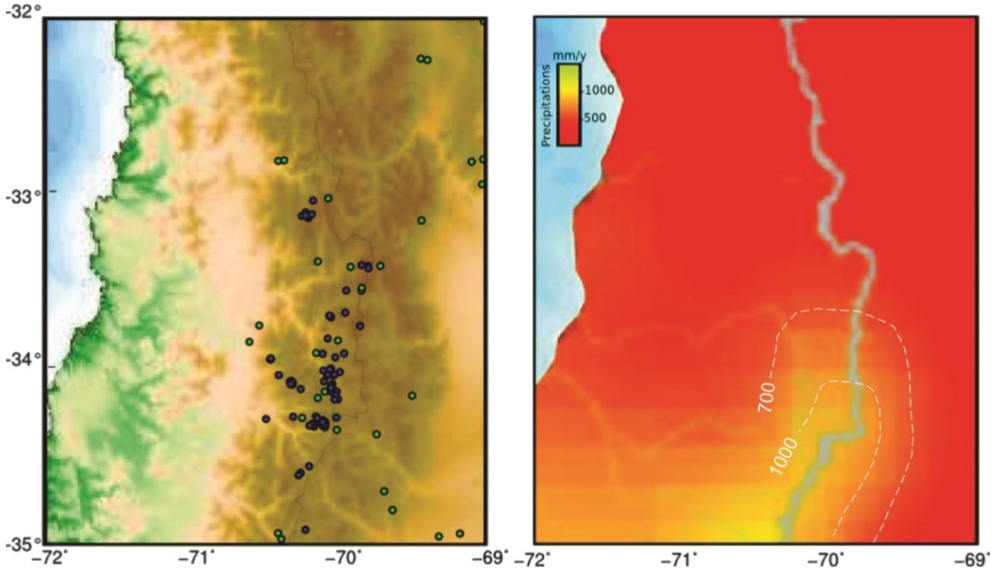


Fig. 9. Detail of the epicenters determined in this work over the western Andean slope south of 33.5°S and relation to rainfall data. Seismic nest coincides with highest precipitation and erosive rates determined in Carretier et al. (2014) in this zone (see Fig. 10).

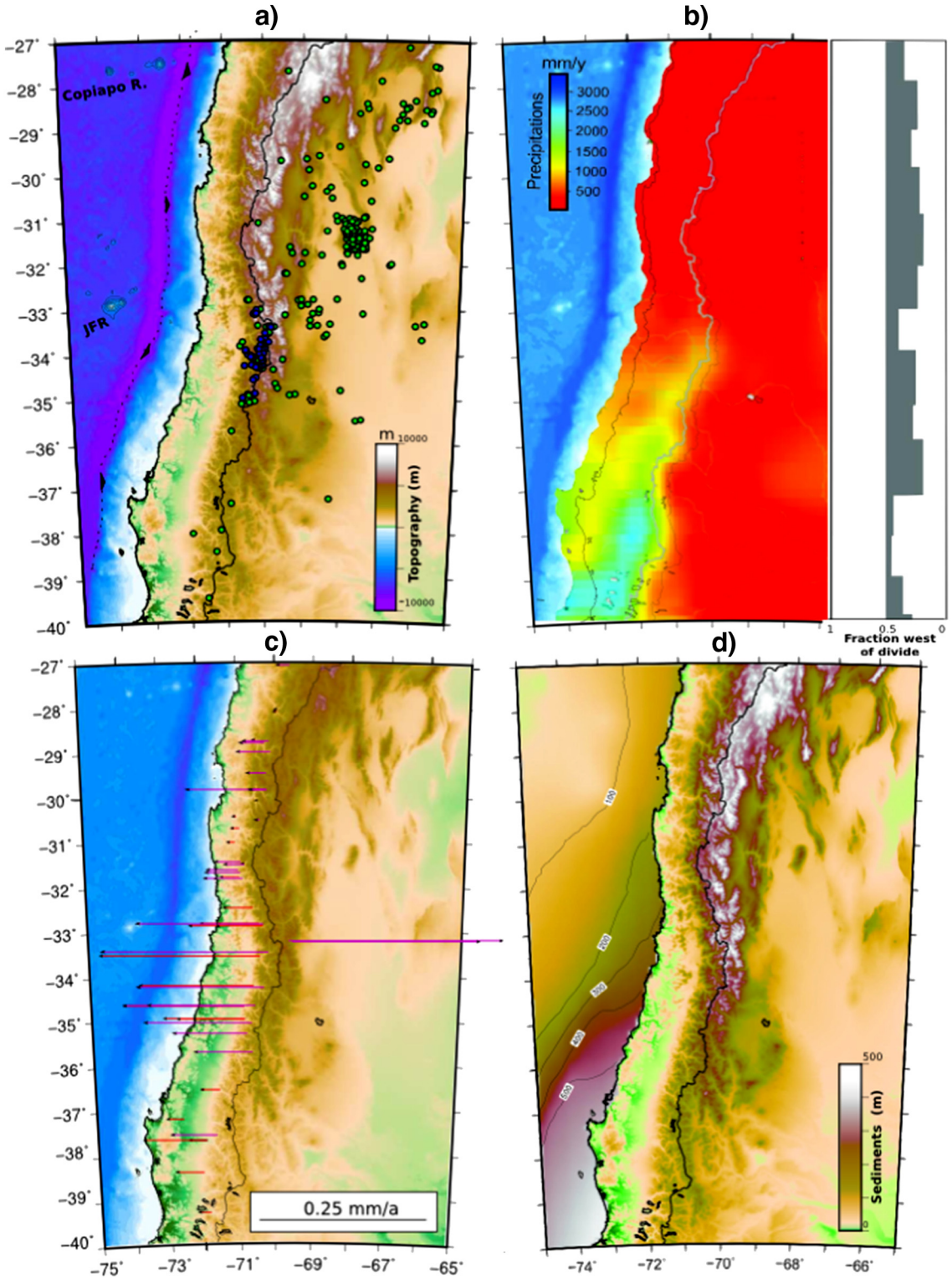


Fig. 10. a) Intraplate shallow seismicity in the transition zone from the Southern Central to the northern Patagonian Andes. Blue and green circles are epicenters located in this work and from EHB bulletin, respectively. b) Precipitation rates from Carretier et al. (2014). c) Red arrows: decadal catchment erosion rates from suspended sediment from Pepin et al. (2010) and Carretier et al. (2014) and violet arrows: millennial catchment-mean erosion rates from ^{10}Be concentration in river sand (Carretier et al., 2013, 2014, Pepin et al., 2010). The scale is indicated by the segment in the lower inset. Catchment areas are not shown here, for detail see Fig. 2 in Carretier et al. (2014). e) Volume of sediments in the trench. Only the sediment thickness scale is shown here, the topography scale is the same than in a). (For interpretation of the references to colour in this figure legend, the reader is referred to the web version of this article.)

References

Alvarado, P., 1998. Sismicidad superficial de los Andes Centrales (33°–35°S; 69.5°–70.5°W). Departamento. Geofísica, Universidad de Chile, p. 161 (Tesis de Magister en Ciencias, mención Geofísica).

Alvarado, P., Barrientos, S., S_aez, M., Astroza, M., Beck, S., 2009. Source study and tectonic implications of the historic 1958 Las Melosas crustal earthquake, Chile, compared to earthquake damage. Phys. Earth Planet. Inter. 175:26–36. http://dx.doi.org/10.1016/j.pepi.2008.03.015.

Alvarez, O., Gimenez, M.E., Martinez, M.P., LinceKlinger, F., Braitenberg, C., 2015a. New insights into the Andean crustal structure between 32° and 34°S from GOCE satellite gravity data and EGM2008 model. In: Sepúlveda, S.A., Giambiagi, L.B., Moreiras, S.M., Pinto, L., Tunik, M., Hoke, G.D., Farías, M. (Eds.), Geodynamic Processes in the Andes of Central Chile and Argentina, Geological Society, London, Special Publications. 399:pp. 183–202. http://dx.doi.org/10.1144/SP399.3.

Alvarez, O., Gimenez, M., Folguera, A., Spagnotto, S., Bustos, E., Baez, W., Braitenberg, C., 2015b. New evidence about the subduction of the Copiapó ridge beneath South America, and its connection with the Chilean-Pampean flat slab, tracked by satellite GOCE and EGM2008 models. J. Geodyn. 91C:65–88. http://dx.doi.org/10.1016/j.jog.2015.08.002.

Amante, C., Eakins, B.W., 2008. ETOPO1 1 arc-Minute Global Relief Model: Procedures, Data Sources and Analysis, National Geophysical Data Center, NESDIS, NOAA. Boulder, CO., U.S. Department of Commerce.

Anderson, M.L., Alvarado, P., Zandt, G., Beck, S., 2007. Geometry and brittle deformation of the subducting Nazca Plate, Central Chile and Argentina. Geophys. J. Int. 171 (1), 419–434.

Araujo, M., Suarez, G., 1994. Geometry and state of stress of the subducted Nazca plate beneath central Chile and Argentina: evidence from teleseismic data. Geophys. J. Int. 116 (2), 283–303.

Barrientos, S., Vera, E., Alvarado, P., Monfret, T., 2004. Crustal seismicity in central Chile. J. S. Am. Earth Sci. 16, 759–768.

Beck, S., Barrientos, S.E., Kausel, E., Reyes, M., 1998. Source characteristics of historic earthquakes along the central Chile subduction zone. J. S. Am. Earth Sci. 11 (2):115–129. http://dx.doi.org/10.1016/S0895-9811(98)00005-4.

Braitenberg, C., Drigo, R., 1997. A crustal model from gravity inversion in Karakorum. Proceedings, International Symposium on Current Crustal Movement and Hazard Reduction in East Asia and South-East Asia, Wuhan, November 4–7, pp. 325–341.

Braitenberg, C., Zadro, M., 1999. Iterative 3D gravity inversion with integration of seismology data: Bollettino di Geophisica Teorica ed Applicata. Proceedings, 2° Joint Meeting IAG, Trieste, v. 40, no. 2.

Braitenberg, C., Pettenati, F., Zadro, M., 1997. Spectral and classical methods in the evaluation of Moho undulations from gravity data: the NE Italian Alps and isostasy. J. Geodyn. 23, 5–22.

Braitenberg, C., Ebbing, J., Götze, H.J., 2002. Inverse modelling of elastic thickness by convolution method-the Eastern Alps as a case example. Earth Planet. Sci. Lett. 202, 387–404.

Braitenberg, C., Wienecke, S., Ebbing, J., Bom, W., Redfield, T., 2007. Joint gravity and isostatic analysis for basement studies-a novel tool. Proceedings, EGM 2007 International Workshop, Innovation on in EM, Grav. and Mag. Methods: A New Perspective for Exploration, Villa Orlandi Capri, Extended Abstracts.

Burd, A.I., Booker, J.R., Mackie, R., Favetto, A., Pomposiello, M.C., 2014. Three dimensional electrical conductivity in the mantle beneath the Matru volcanic field in the Andean back-arc of Argentina Payun near 36.5° S: decapitation of a mantle plume by resurgent upper mantle shear during slab steepening? Geophys. J. Int. 1, 1–12.

Cahill, T., Isacks, B.L., 1992. Seismicity and shape of the subducted Nazca plate. J. Geophys. Res. 97 (B12), 17503–17529.

Carretier, S., Regard, V., Vassallo, R., Aguilar, G., Martinod, J., Riquelme, R., Pepin, E., Charrier, R., Hérail, G., Farías, M., Guyot, J.-L., Vargas, G., Lagane, C., 2013. Slope and Climate Variability Control of Erosion in the Andes of Central Chile Geology. 41 (2) pp. 195–198.

Carretier, S., Tolorza, V., Rodríguez, M.P., Pepin, E., Aguilar, G., Regard, V., Martinod, J., Riquelme, R., Bonnet, S., Brichau, S., Hérail, G., Pinto, L., Farías, M., Charrier, R., Guyot, J.L., 2014. Erosion in the Chilean Andes between 27°S and 39°S: tectonic, climatic and geomorphic control. In: Sepúlveda, S.A., Giambiagi, L.B., Moreiras, S.M., Pinto, L., Tunik, M., Hoke, G.D., Farías, M. (Eds.), Geodynamic Processes in the Andes of Central Chile and Argentina. Geological Society, London, Special Publications.

Christensen, D., Ruff, L., 1986. Rupture process of the March 3, 1985 Chilean earthquake. Geophys. Res. Lett. 13 (8), 721–724.

Cornejo, P., Mahood, G., 1997. Seeing past effects of re-equilibration to reconstruct magmatic gradients in plutons: La Gloria Pluton, central Chilean Andes. Contrib. Mineral. Petrol. 127, 159–175.

Crotwell, H.P., Owens, T.J., 1998. The TauP Toolkit: Flexible Seismic Travel-time and Raypath Utilities Version 2.0. Department of Geological Sciences, University of South Carolina.

Dadson, S.J., Hovius, N., et al., 2003. Links between erosion, runoff, variability and seismicity in the Taiwan orogeny. Nature 426, 648–651.

Ebbing, J., Braitenberg, C., Wienecke, S., 2007. Insights into the lithospheric structure and tectonic setting of the Barents Sea region from isostatic considerations. Geophys. J. Int. 171, 1390–1403.

Engdahl, E.R., van der Hilst, R., Buland, R., 1998. Global teleseismic earthquake relocation with improved travel times and procedures for depth determination. Bull. Seismol. Soc. Am. 88, 722–743.

Farías, M., 2007. Tectonique, erosion et evolution du relief dans les Andes du Chile Central au cours du neogene. Tesis Doctoral. Universite Toulose III, Santiago de Chile 238 p.

Farías, M., Charrier, R., Carretier, S., Martinod, J., Fock, A., Campbell, D., Cáceres, J., Comte, D., 2008. Late Miocene high and rapid surface uplift and its erosional response in the Andes of Central Chile (33°-35°S). Tectonics 27 (1). http://dx.doi.org/10.1029/2006TC002046.

Fock, A., 2005. Cronología y tectónica de la exhumación en el neógeno de los Andes de Chile Central entre los 33° y los 34° S. Tesis Grado Magister, Universidad de Chile, Facultad de Ciencias Físicas y Matemáticas, Santiago de Chile 235 p.

Folguera, A., Ramos, V.A., 2009. Collision of the mocha fracture zone and a < 4 Ma old wave of orogenic uplift in the Andes (36°–38° S). Lithosphere 1:364–369. http://dx.doi.org/10.1130/L66.1.

Folguera, A., Alvarado, P., Arriagada, C., Ramos, V., 2015. Tectonics of the Argentine and Chilean Andes: an introduction. J. S. Am. Earth Sci.

Gansser, A., 1973. Facts and theories on the Andes. J. Geol. Soc. Lond. 129, 93–131.

Giambiagi, L., Tunik, M., Barredo, S., Bechis, F., Ghiglione, M., Alvarez, P., Drosina, M., 2009. Cinemática de apertura del sector norte de la Cuenca Neuquina. Rev. Asoc. Geol. Argent. 65 (2), 278–292.

Giambiagi, L., Tassara, A., Mescua, J., Tunik, M., Alvarez, P.P., Godoy, E., Hoke, G., Pinto, L., Spagnotto, S., Porras, H., Tapia, F., Jara, P., Bechis, F., García, V.A., Suriano, J., Moreiras, S.M., Pagano, S.D., 2014. Evolution of shallow and deep structures along the Maipo–Tunuyán transect (33°40′S): from the Pacific coast to the Andean foreland Geological Society. 399. Special Publications, London. http://dx.doi.org/10.1144/SP399.14.

Gimenez, M.E., Martínez, M.P., Introcaso, A., 2000. A Crustal Model based mainly on gravity data in the area between the Bermejo Basin and the Sierras de Valle Fértil – Argentina. J. S. Am. Earth Sci. 13, 275–286.

Gimenez, M.E., Braitenberg, C., Martinez, M.P., Introcaso, A., 2009. A Comparative Analysis of Seismological and Gravimetric Crustal Thicknesses below the Andean Region with Flat Subduction of the Nazca Plate. Journal of GeophysicsHindawi Publishing Corporation International (Article ID 607458, 8 p). 10.1155/2009/607458.

Hardebeck, J., Shearer, P., 2002. A new method for determining first motion focal mechanisms. Bull. Seismol. Soc. Am. 92 (6), 2264–2276.

Hardebeck, J., Shearer, P., 2005. HASH: A FORTRAN Program for Computing earthquake First Motion Focal Mechanisms – v1.1.

Havskov, J., Ottemöller, L., Canabrava, R.L.P., 2007. SEISAN: multiplatform implementation of MINISEED/SEED. Orfeus Newsletter 7 (2).

Hervé, F., Munizaga, F., Parada, M.A., Brook, M., Pankhurst, R.J., Snelling, N.J., Drake, R., 1988. Granitoids of the coastal range of central Chile: geochronology and geologic setting. J. S. Am. Earth Sci. 1, 185–194.

Hervé, F., Greene, F., Pankhurst, R.J., 1994. Methamorphosed fragments of oceanic crust in the upper Paleozoic Chonos accrecionary complex, southern Chile. J. S. Am. Earth Sci. 7 (3/4), 263–270.

Hildreth, W., Moorbath, S., 1988. Crustal contributions to arc magmatism in the Andes of Central Chile. Contrib. Mineral. Petrol. 98 (4), 455–489.

Introcaso, A., Pacino, M.C., Guspi, F., 2000. The Andes of Argentina and Chile: crustal configuration, isostasy, shortening and tectonic features from gravity data. Temas de Geociencia 5, 31.

Isacks, B., Jordan, T.E., Allmendinger, R., Ramos, V.A., 1982. La segmentación tectónica de los Andes Centrales y su relación con la placa de Nazca subductada. V Congreso Latinoamericano de Geología, Actas, 111, 587–606. Aires, Buenos.

Kay, S.M., Maksaev, V., Moscoso, R., Mpodozis, C., Nasi, C., 1987. Probing the evolving Andean lithosphere: mid-late tertiary magmatism rocks in Chile (29°–30°30′S) over the modern zone of subhorizontal subduction. J. Geophys. Res. 92 (B7), 6173–6189.

Kay, S., Godoy, E., Kurtz, A., 2005. Episodic arc migration, crustal thickening, subduction erosion, and magmatism in the south-central Andes. GSA Bull. 117 (1–2), 67–88.

Kendrick, E., Bevis, M., Smalley, R.J., Brooks, B.A., Barriga, R., Lauría, E., Souto, L.P., 2003. The Nazca-South America Euler vector and its rate of change. J. S. Am. Earth Sci. 16 (2), 125–131.

Kilb, D., Hardebeck, J., 2006. Fault parameter constraints using relocated earthquakes: a validation of first-motion focal-mechanism data. Bull. Seismol. Soc. Am. 96 (3), 1140–1158.

Lange, D., Tilmann, F., Barrientos, S.E., Contreras-Reyes, E., Methe, P., Moreno, M., Heit, B., Agurto, H., Bernard, P., Vilotte, J.P., Beck, S., 2012. Aftershock seismicity of the 27 February 2010 Mw 8.8 Maule earthquake rupture zone. Earth Planet. Sci. Lett. 317–318, 413–425.

Liener, B.R., Havskov, J., 1995. A computer program for locating earthquakes locally, regionally and globally. Seismol. Res. Lett. 66, 26–36.

Maurer, V., Kissling, E., Husen, S., Quintero, R., 2010. Detection of systematic errors in travel-time data using a minimum 1D model: application to Costa Rica seismic tomography. Bull. Seismol. Soc. Am. 100 (2), 629–639.

Miranda, S., Robles, J.A., 2002. Posibilidades de atenuacion cortical en la cuenca Cuyana a partir del analisis de datos de gravedad. Revista de la Asociacion Geologica Argentina 57, 271–279.

Moreno, M.S., Bolte, J., Klotz, J., Melnick, D., 2009. Impact of megathrust geometry on inversión of coseismic slip from geodetic data: application to the 1960 Chile earthquake. Geophys. Res. Lett. L16310 (36). http://dx.doi.org/10.1029/2009GL039276.

Mpodozis, C., Cornejo, P., 2012. Cenozoic Tectonics and Porphyry Copper Systems of the Chilean Andes. Soc. Econ. Geol. Spec. Pub. 16, 329–360.

Nacif, S., Triep, E., Spagnotto, S., Aragon, E., Furlani, R., Álvarez, O., 2015. The flat to normal subduction transition study to obtain the Nazca plate morphology using high resolution seismicity data fromthe Nazca plate in Central Chile. Tectonophysics 657 (2015), 102–112.

Oldenburg, D., 1974. The inversion and interpretation of gravity anomalies. Geophysics 39, 526–536.

Pardo, M., Comte, D., Monfret, T., 2002. Seismotectonic and stress distribution in the central Chile subduction zone. J. S. Am. Earth Sci. 15 (1), 11–22.

Parker, R.L., 1972. The rapid calculation of potential anomalies. Geophys. J. R. Astron. Soc. 31, 447–455.

Pavlis, N.K., Holmes, S.A., Kenyon, S.C., Factor, J.K., 2008. An earth gravitational model to degree 2160: EGM2008. Proceedings, General Assembly of the European Geosciences Union: Vienna, Austria, p. 2008.

Pavlis, N.K., Holmes, S.A., Kenyon, S.C., Factor, J.K., 2012. The development and evaluation of the Earth gravitational model 2008 (EGM2008). J. Geophys. Res. 117 (B04406). http://dx.doi.org/10.1029/2011JB008916.

Pepin, E., Carretier, S., Guyot, J.L., Escobar, F., 2010. Specific suspended sediment yields of the Andean rivers of Chile and their relationship to climate, slope and vegetation. Hydrological Sciences Journal – Journal des Sciences Hydrologiques 55 (7), 2010.

Perez-Gussinyé, M., Lowry, A.R., Phipps Morgan, J., Tassara, A., 2008. Effective elastic thickness variations along the Andean margin and their relationship to subduction geometry. Geochem. Geophys. Geosyst. 9, Q02003.

Persson, K.S., Sokoutis, D., 2002. Analogue models of orogenic wedges controlled by erosion. Tectonophysics 356, 323–336.

Pesicek, J.D., Engdahl, E.R., Thurber, C.H., DeShon, H.R., Lange, D., 2012. Mantle subducting slab structure in the region of the 2010 M8.8 Maule earthquake (30–40°S), Chile. Geophys. J. Int. 191, 317–324.

Ramos, V., Cristallini, E.O., Perez, D.J., 2002. The pampean flat-slab of the Central Andes. J. S. Am. Earth Sci. 15, 59–78.

Rodi, W., 2006. Grid-search event location with non-Gaussian error models. Phys. Earth Planet. Inter. 158, 55–66.

Rojas Vera, E.A., Sellés, D., Folguera, A., Gímenez, M., Ruiz, F., Orts, D., Zamora, G., Valcarce, Martínez P., Bechis, F., Ramos, V.A., 2014. The origin of the Loncopúe trough in the retroarc of the southern Central Andes from field, geophysical and geochemical data. Tectonophysics 637, 1–19.

Ruiz, S., Grandin, R., Dionicio, V., Satriano, C., Fuenzalida, A., Vignyc, C., Kiraly, E., Meyer, C., Baez, J.C., Riquelme, S., Madariaga, R., Campos, J., 2013. The Constitución earthquake of 25 March 2012: a large aftershock of the Maule earthquake near the bottom of the seismogenic zone. Earth Planet. Sci. Lett. 377–378, 347–357.

Sacek, V., Ussami, N., 2009. Reappraisal of the effective elastic thickness for the sub-Andes using 3-D finite element flexural modelling, gravity and geological con- straints. Geophys. J. Int. 179, 778–786.

Sagripanti, L., Rojas Vera, E.A., Gianni, G., Folguera, A., Harvey, J., Farías, M., Ramos, V., 2015. Neotectonic reactivation of the western section of the Malargüe fold and thrust belt Tromen volcanic plateau, Southern Central Andes. Geomorphology 232 (2015), 164–181.

Sbar, M.L., Barazangi, M., Dorman, J., Scholz, C.H., Smith, R.B., 1972. Tectonics of the intermountain Seismic Belt, western United States, Microearthquake seismicity and composite fault plane solutions. Geol. Soc. Am. Bull. 83, 13–28.

Snoke, J.A., Munsey, J.W., Teague, A.G., Bollinger, G.A., 1984. A program for focal mechanism determination by combined used of polarity and SV-P amplitude ratio data. Earthq. Notes 55, 15.

Stewart, J., Watts, A.B., 1997. Gravity anomalies and spatial variations of flexural rigidity at mountain ranges. J. Geophys. Res. 102, 5327–5352.

Syracuse, E.M., Abers, G.A., 2006. Global compilation of variations in slab depth beneath arc volcanoes and implications. Geochem. Geophys. Geosyst. 7 (5). http://dx.doi.org/10.1029/2005GC001045.

Tassara, A., 2005. Interaction between the Nazca and South American plates and formation of the Altiplano–Puna plateau: review of a flexural analysis along the Andean margin (158–348S). Tectonophysics 399, 39–57.

Tassara, A., Yáñez, G., 2003. Relación entre el espesor elástico de la litósfera y la segmentación tectónica del margen Andino (15–47°S). Rev. Geol. Chile 30, 159–186.

Tassara, A., Swain, C., Hackney, R., Kirby, J., 2007. Elastic thickness structure of South America estimated using wavelets and satellite-derived gravity data. Earth Planet. Sci. Lett. 253, 17–36.

Vening-Meinesz, F.A., 1939. Tables Fondamentales pour la Reduction Isostatique Regionale. Bulletin Géodésique 63, 711–776.

Wienecke, S., 2006. A new analytical solution for the calculation of flexural rigidity: significance and applications. PhD Thesis. Free University Berlin, Berlin 126 p.. (World Wide Web Address:). http://www.diss.fuberlin.de.

Wienecke, S., Braitenberg, C., Göetze, H.J., 2007. A new analytical solution estimating the flexural rigidity in the Central Andes. Geophys. J. Int. 169, 789–794.

Yáñez, G., Cembrano, J., Pardo, M., Ranero, C., Selles, D., 2002. The challenger-Juan Fernandez-Maipo major tectonic transition of the Nazca-Andean subduction system at 33–34° S: geodynamics evidence and implications. J. S. Am. Earth Sci. 15, 23–38.

Zadro, M., Braitenberg, C., 1997. Spectral methods in gravity inversion: the geopotential field and it's derivatives. Annali di geofisica XL 5, 1433–1443.